ORNL-4811

# Health Physics DIVISION



## Annual Progress Report

### Period Ending July 31, 1972

OAK RIDGE NATIONAL LABORATORY
OPERATED BY UNION CARBIDE CORPORATION • FOR THE U.S. ATOMIC ENERGY COMMISSION

# Contents

# Summary

## PART I. RADIATION PHYSICS

### 1. Theoretical Radiation Physics

A theoretical study has been made of the energy deposited in water spheres and cylinders of various sizes around the site at which an oxygen or carbon nucleus captures a stopped negative pion. A review has been made of methods for calculating the spectra of delta rays produced by heavy ions and electrons, with a view toward their incorporation into microdosimetry theory. Calculations have been made of electron-slowing-down spectra in semiconductors based on the use of model cross sections for the valence band in a semiconductor and classical cross sections for excitations from inner levels. Interesting new formulas have been obtained for the inner-shell excitation of atoms by slow heavy charged particles, using the perturbed stationary state formalism of Mott. An extensive theoretical study of the effects of dipolar forces on charged-particle scattering phenomena has been made. Use has been made of Feshbach's elegant and powerful technique for determining elastic and total scattering cross sections under multichannel scattering conditions in an application to atomic scattering of electrons above the ionization potential of the target. Very satisfactory results for elastic and total scattering cross sections have been obtained for electrons on hydrogen. The mean free path of an electron in a nearly free electron gas has been investigated, yielding a result which predicts an appreciable probability for plasmon excitation by an incident electron with energy well below the threshold predicted by the usual zero-damping theory. A general review has been made of some of the interesting properties of plasmons and their manifestations in experimental physics. We have obtained analytical expressions which may be used to relate the damping of long-wavelength plasma waves to experimentally determined values of the complex dielectric permittivity of a medium. We have shown that the classical image potential outside a metal may be considered to originate in the shifted zero-point energy of the surface plasmon field and that retardation correction to this potential gives a more rapid falloff with the distance than predicted by the classical theory at distances which are of the order of tens to hundreds of angstroms from the surface, depending upon the quantum plasma energy of the metal.

### 2. Interaction of Radiation with Solids and Liquids

Measurements of the optical properties of a medium can yield information about the modes of energy deposition occurring when high-energy charged particles or electromagnetic radiation interact with the medium. Thus we have a continuing program to measure and interpret the optical properties of materials of basic importance. During this year the optical constants of K have been measured above the plasma energy and the results compared with those obtained previously for Na, Rb, and Cs. The most plausible explanation for the strong absorption seen above the plasma energies in all these alkali metals is that of plasmon-assisted interband transitions. The optical properties of glassy carbon have been obtained up to 82 eV and interpreted, by comparison with graphite, in terms of $\pi$ and $\sigma$ single-electron transitions and collective oscillations. In addition, work function changes during oxygen chemisorption on fresh Mg surfaces have been correlated with the observed exoelectron emission. A method has been developed for obtaining extinction coefficients from critical angle measurements which gives greater accuracy than the usual method of fitting Fresnel's equations for reflectance as a function of angle of incidence. A technique has also been developed for revitalizing vacuum ultraviolet diffraction gratings.

### 3. Physics of Tissue Damage

The experimental investigation of the electron-slowing-down spectra in semiconductors was completed with a study of silicon. The shape of the spectrum was similar to that of germanium and of those conductors studied earlier, but did show some evidence of discontinuities near the silicon $L$- and $K$-shell energies.

These are attributed to electron-induced ionizations of the shells.

Electron-slowing-down studies have been extended to include insulating materials. Preliminary data have been obtained using aluminum oxide doped with a small amount of dysprosium, which served as the electron source. Electron fluxes were found to be generally higher than those for a typical conductor.

A series of studies was initiated on the influence of source thickness on the slowing-down spectra in an effort to explain the present discrepancy between theory and experiment. In the thinner sources a pronounced peak in the electron flux was observed at the *LMM* Auger range. This represents a new source which can contribute to the electron flux at lower energies and may be, in part, responsible for the poor agreement between theory and experiment at the lower energies.

Experimental studies of the optical properties of organic liquids was continued with investigations of several commonly used solvents. The measurements were made using a newly developed transmission cell which enables studies to be carried out on samples as thin as 500 Å.

An experimental investigation of the optical and dielectric properties of the nucleic acid bases has been initiated. Preliminary data have been obtained for guanine at energies up to 80 eV which, in general, show good agreement with the results of the electron-energy-loss studies obtained by scanning electron microscope techniques.

### 4. Electron and Ion Collision Physics

The first experimental values for thermal and near-thermal electron transport coefficients have been determined for oxygen and water vapor with a time-of-flight electron swarm experiment using the drift-dwell-drift technique. Comparison with theory where available is good. Studies of the interaction of low-energy electrons with a series of organic and organometallic compounds in the gas phase have elucidated a number of new electron-molecule reaction mechanisms. Electron collisions with a series of anhydride molecules produced metastable $CO_2^{-*}$ ions, and the lifetime of this ion was measured for the first time. Also, metastable ions of the form $C_xH_yCO_2^{-*}$ were found to dissociate after electron detachment into energetic $C_xH_y$ and $CO_2$ molecules. The formation of positive and negative ions in the organometallic "sandwich" compounds ferrocene, cobaltocene, nickelocene, and magnesocene have been studied by high-resolution electron impact mass spectrometry techniques. The electron affinities of a number of organic and inorganic molecules have been determined by the cesium collisional ionization technique. A number of positive-ion condensation reactions in the benzene system have been examined in a time-of-flight mass spectrometer. Ion-pair production by chemi-ionizing collisions of exicted rare-gas atoms with molecules have been studied and show extremely large cross sections. In short, a number of gas collision problems of direct interest to radiation chemistry have been studied.

### 5. Atomic and Molecular Radiation Physics

Intermediate phase studies for understanding radiation interaction with condensed media and for developing a coherent picture of radiation interaction with matter are discussed with emphasis on electron attachment and drift through low- and high-pressure gases and liquids. Highlights of our studies on long-lived polyatomic negative ions, moderately short-lived negative ions, compound negative-ion resonance states, threshold-electron excitation of polyatomic molecules, and thermal electron scattering by molecules are outlined. The emphasis in these studies is on key groups of organic molecules including O- and $NO_2$-containing organic molecules, *N*-heterocyclic benzene and naphthalene derivatives, and saturated and aromatic hydrocarbons. Reactions of molecular Rydberg states and emission spectra from higher excited $\pi$-singlet states of aromatic hydrocarbons in solution are also discussed.

### 6. Graduate Education and Vocational Training

The health physics training program included fellowship students from the University of Kentucky, the University of Michigan, Georgia Institute of Technology, and Purdue University. These reported to ORNL for summer on-the-job instruction in applied and research health physics.

Division personnel visited eight colleges and universities to give seminars on various research problems of current interest and also to help recruit qualified students in the fellowship program.

The Health Physics Division provided research facilities and advisors for 13 Oak Ridge Graduate Fellows, AEC Fellows, and USPHS Fellows who were conducting thesis research.

Teaching assistance was given to The University of Tennessee for its program in radiation physics. Lectures

and tours were given for several university groups visiting ORNL.

Assistance and consultation were given to six schools that were interested in establishing health physics courses or programs in their science departments.

The Division cooperated with ORAU in the presentation of a ten-week course in applied health physics and in the screening of applicants for AEC Fellowships.

## PART II. RADIATION DOSIMETRY RESEARCH

### 7. Dosimetry for Human Exposures and Radiobiology

Calculations of dose distributions in human-size tissue-equivalent phantoms for a wide variety of radiation sources continues to be a major objective in this research. During this report period, emphasis was again placed on distributions from $^{252}Cf$, monoenergetic neutrons incident at 45° with the axis of the phantom, and monoenergetic photons incident unilaterally on a heterogeneous phantom. Local dose distributions for implanted $^{252}Cf$ sources were determined, and tables of exposure values were prepared for regions close to the source. Neutron isodose curves in tissue were also prepared. An absolute comparison of measured dose distributions (reported in ORNL-4720) was made with calculations. The agreement was found to be within the probable errors of measurement and calculation. Values of neutron and gamma-ray dose were measured in the vicinity of a $^{252}Cf$ source facility within the Biology Division. This was done to determine the exposure conditions for specimens irradiated at that facility. Liaison with the Atomic Bomb Casualty Commission has continued. Studies of particular importance include dosimetry for "heavy shielding" cases, determinations of organ doses, and a pilot study of the histories of survivors who were exposed to the radioactive "black rain."

### 8. Applied Dosimetry Research

Major emphasis in the solid-state dosimetry program continues to be in the area of detector research. Exoelectron emission studies were centered around the role and nature of activators in the ceramic BeO detectors, reproducibility of TSEE readout, stability of stored signals, effects on TSEE response such as atmospheric, temperature, light, etc., and the development of TSEE readers. TSEE activators such as sodium, lithium, magnesium, and aluminum were added to ceramic BeO before firing to 1600°C. None of these samples exhibited a glow curve different from that of BeO 995, which has a natural content of silicon of 2000 ppm. These activators seem to promote exoelectron emission which is already intrinsic to the ceramic BeO by increasing the efficiency of exoelectron release. A significant fading study was made of a variety of new solid-state detectors as well as several film dosimeters. It was found that latent unetched fission fragment tracks in 10-μm polycarbonate foil are stable for at least three months at 30°C and 95% relative humidity. Radiophotoluminescent (RPL) and thermoluminescent (TLD) detectors as well as common dosimeter films were included in this study. Three different RPL dosimeters showed less than 15% deviation in readings between one day and three months after exposure if stored at 30°C and 95% relative humidity. Of various TL detectors, fading in $CaSO_4$:Dy was barely detectable, while $CaF_2$:Dy showed pronounced fading under the same conditions. Studies associated with developing an alternative detector (to photographic film) for personnel neutron monitoring have continued and were centered on the registration of charged particles in plastic.

### 9. Interaction of Charged Particles with Matter

The specific objective of this research program continues to be directed at determining energy pathways after swift charged particles interact with gases. During this report period studies have centered on the interaction of 2-MeV protons with helium at pressures between $10^{-3}$ and $10^{3}$ torr. The dominating ($2^1P$) state was studied by observing the time behavior of a resonance line resulting from $2^1P$-$1^1S$ transitions at 584 Å. Comparing these data with the intensity and time behavior of the continuous emission, it was concluded that the atomic state $2^1P$ is converted to two different excited molecular states in helium by three-body collisions. The energy pathways model developed in these studies suggests that the Jesse effect originates from a metastable molecule rather than from an atomic state, as previously believed. An operational rationale for radiation protection is being developed which is not encumbered by such concepts as "permissible levels" measured in terms of absorbed dose or its myriad of factors. The radiation field is defined by specifying every variable which could considerably affect the biological probabilities. Two approaches to the problem are being pursued. In the first approach an operational relationship between radiation and effect is expressed by assuming that an operator exists which transforms the radiation field directly into probabilities of ob-

serving effects. The second approach embodies an operational relationship implied in the first approach and prompted by the observation that there are no "radiation diseases." The objective here is to discover the operator $O(N)$ which changes the natural rate of incidence to that which occurs as a result of radiation ($N$). A joint program with the Biology Division is under way in which an attempt is being made to find the operator $O(N)$ for the case of mouse cataract incidence.

### 10. HPRR Accelerator Operations

The HPRR continues to provide a reliable and versatile irradiation facility. During this report period it was opearated without fault in support of a dozen different types of experiments for representatives of foreign countries, many colleges and universities, Federal contractors and licensees, and other agencies. In July 1972, the ninth in a series of intercomparisons of nuclear accident dosimeters was conducted. Participants included AEC contractors and companies holding licenses for handling large quantities of fissile material.

In support of the program in nuclear safety, an extensive calculation of the HPRR's neutron energy spectra under three different conditions was made. A comparison of these calculations with previous measurements has been completed. The close agreement promotes a feeling of confidence in the calculations. The 3-MV Van de Graaff was operated throughout this report period in support of the energy pathways studies. Dosimetry studies and the determination of detector responses were performed using the DOSAR Low-Energy Accelerator.

### 11. Spectrometry Research and Development

New applications of previously developed techniques highlighted the work in spectrometry research. For example, the capabilities developed for the zone refining of organic scintillators were applied to other organic compounds being studied by mass spectroscopy in the Radiation Physics Section. Instrument development produced a stable source of light pulses for use as a standard in the organic scintillator studies and a paper-tape-to-typewriter translator that rejects nonsignificant zeros to aid in the clarity of a digital readout. Two different fast-neutron detectors with high sensitivity were developed. The first was for use with the Aerial Radiological Measuring Surveys system operated for the Atomic Energy Commission by the Las Vegas Division of EG&G, Inc. The second was a fast-neutron spectrometer for measuring neutrons with energies above 200 keV as a function of incident angle on the roof of the DOSAR Control Building during HPRR operations. These data are part of a program to evaluate the doses received by survivors in heavy-shielding buildings at Hiroshima and Nagasaki. An increasing commitment to studying radiation in the environment was expressed by the development of a computer program to calculate possible isotope concentrations produced in the environment by the operation of a power reactor. High-resolution gamma-ray and alpha-particle spectrometers were obtained and put into use for measuring natural radioactivity, particularly in situations where it is higher than average. A new program was begun to measure the distribution of stopping of low-energy protons in tissue-constituent elements, data that are of general value for dosimetry calculations.

## PART III. INTERNAL DOSIMETRY

### (Chapters 12–16)

Estimation of absorbed fractions of photon energy per gram of target organ is of great importance, since dose is proportional to this quantity and for many organs of the body, particularly the gonads, the direct Monte Carlo calculation is inaccurate. The accuracy of the estimates obtained in the report "Estimates of Absorbed Fractions for Photon Emitters within the Body" are generally well within the range expected of most dose estimates, particularly when the organ involved receives only a small fraction of the dose to the critical organ or tissue. It is hoped that this method of using the buildup factor in obtaining estimates of dose will come into general use.

The second report on "Estimates of Dose to Infants and Children from a Photon Emitted in the Lungs" is likewise an extension of previous work. It appears that the dose to the child per photon is frequently higher than for an adult, the difference being one to two orders of magnitude. The extension of these results to other source organs poses problems of great interest for clinical use of nuclear energy as well as for estimates of dose due to exposure of the population.

The study of the metabolism of magnesium and its dosimetry is one example among many of the models constructed for estimation of dose needed for the revision of ICRP Publication 2. It will be circulated for review by the ICRP.

The remaining reports on blood volume in lungs and on excretion of plutonium are examples of the continuing need for metabolic data on the behavior of radionuclides in the body and of their importance for estimation of dose.

## PART IV. ENVIRONMENTAL STUDIES

### 17. Dose Estimation Studies Related to Peaceful Uses of Nuclear Explosives and Other Radionuclide Releases

Research continued on development of the CUEX methodology for assessing radiation exposures of human populations via all important exposure pathways for environmental releases of radioactivity. Methods developed under this activity were used to complete radiological sections of environmental impact statements (utility-owned nuclear power stations) prepared at ORNL for the AEC to meet the requirements of the National Environmental Policy Act of 1969. Dose estimates were made for all significant exposure pathways following a careful study of the nuclear power station and its environment. Radiation doses, both to individuals and to total population within 50 miles of the station, were estimated. Comparisons were made of the estimated doses with the appropriate radiation safety guides and the doses due to natural background radiation.

The radioactivity release experience of light-water power reactors was analyzed in a number of ways to identify critical aquatic exposure pathways and critical radionuclides. This work was a supporting effort to the above-mentioned application of CUEX methodology. The radionuclides given consideration in the analysis were those which satisfied several criteria thought to be indicative of possible environmental impact. The work provided a standard list of radionuclides which should be considered in estimating the environmental impact of radioactivity released in the liquid effluent of current light-water power reactors.

Work on dose estimations related to the Gasbuggy project, the first experiment performed to demonstrate the feasibility of using nuclear explosives to increase production of natural gas, was completed with the preparation of three topical reports. Tritium behavior in a natural gas processing plant was studied as a part of the evaluation of consumer products from Project Gasbuggy. Data obtained during the study experiment indicate that the projected whole-body doses to plant workers, attributable to tritium releases during processing of nuclearly stimulated gas, would be less than 1% of the dose from natural background radiation. The observed distribution of tritium among plant products confirmed theoretical calculations, lending confidence in our ability to predict the quantities of radioactivity in gas and liquid products leaving a plant that processes gas from nuclearly stimulated wells.

The first phase of Rulison (the second experiment performed to demonstrate the feasibility of using nuclear explosives to increase production of natural gas) dose estimations considered the radiological impact of hypothetical introduction of gas from the Rulison well into the distribution systems of two small gas transmission systems located near the well site. Inhalation and skin absorption of tritium dispersed in the atmosphere gave doses less than 1 millirem per year, but home exposure to unvented combustion products from kitchen ranges, the critical exposure pathway, could have given a dose of 3.0 millirems per year in one system and up to 20 millirems per year in the system that provided very little dilution of the Rulison gas. Computer programs were developed to aid estimation and control of doses from natural gas produced in a nuclearly stimulated well field.

# 15. A Metabolic Model for Magnesium in Man and an Estimate of Dose to Bone and Soft Tissue Resulting from a Single Intravenous Injection of $^{28}Mg$

S. R. Bernard

The metabolic model of Avioli and Berman,[1] based on measurements of blood, urine, and feces of 15 human subjects who had been administered tracer doses of $^{28}MgCl_2$ intravenously, appears in Fig. 15.1. Compartments 1, 2, 3, and 4 are "body" compartments, with 1 representing blood and 2, 3, and 4 only stated to be extravascular compartments. Avioli and Berman did not identify the other three body compartments, because they only had measurements on blood and excreta. These data only yield the four eigenvalues of the 4 × 4 matrix of rate transfer constants and some information on the constraints on the λ's. To estimate all $4^2$ rate transfer constants uniquely, data are needed on all four compartments. Further details on the uniqueness of compartment models may be found in the paper by Berman and Schoenfeld.[2] The arrow pointing down from compartment 1 represents excretion. The starred arrow identifies the site of the initial $^{28}Mg$ injection. The $\lambda_{ij}$'s are the rate transfer constants given by Avioli and Berman. These values appear in Fig. 15.1. Although Avioli and Berman give ranges of values and standard deviations, the present model uses only the means. The dashed arrow from compartment 4 to 3 indicates that this pathway connection was not observed directly but was estimated from literature data on stable Mg levels in bone and muscle and with the tracer data.

In estimating internal dose, equations for retention in organs and tissues and total body are needed. From the data in Fig. 15.1, the linear differential equations for the "body" compartments of the model of Avioli and Berman, written in matrix form, are:

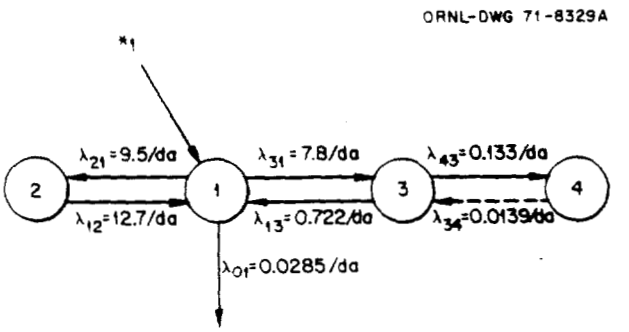


**Fig. 15.1. Berman's compartmental model assumed for $^{28}Mg$ analysis.** Compartment 1 refers to ultrafilterable plasma Mg; compartments 2, 3, and 4 represent extravascular compartments. Compartment 4 is depicted as a slowly exchanging magnesium pool postulated to exist under steady-state conditions with slow turnover rate ($\lambda_{34}$).

The time $t$ is expressed in days. Here $y_i(t)$ ($i$ = 1, 2, 3, 4) corresponds to the amount present in compartment $i$ at time $t$, and $\dot{y}_i(t)$ is the derivative $dy_i(t)/dt$. A computer code written by J. A. Carpenter, ORNL Mathematics Division, was used to obtain the solutions of (1). These appear in Eq. (2), which is also in matrix form, and apply to the case of unit intake into compartment 1 at zero time. Here $Y(t)$ stands for the column vector of $y_i(t)$, $i$ = 1, 2, 3, 4. Equation (3)

$$\dot{Y}(t) = \begin{pmatrix} \dot{y}_1(t) \\ \dot{y}_2(t) \\ \dot{y}_3(t) \\ \dot{y}_4(t) \end{pmatrix} = - \begin{pmatrix} 17.8 & -12.7 & -0.722 & -0.0 \\ -9.5 & 12.7 & -0.0 & -0.0 \\ -7.8 & -0.0 & 0.855 & -0.0139 \\ -0.0 & -0.0 & -0.133 & 0.0139 \end{pmatrix} \begin{pmatrix} y_1(t) \\ y_2(t) \\ y_3(t) \\ y_4(t) \end{pmatrix} \quad (1)$$

1. L. V. Avioli and Mones Berman, "$^{28}Mg$ Kinetics in Man," *J. Appl. Physiol.* 21(6), 1688–94 (1966).
2. M. Berman and R. Schoenfeld, "Invariants in Experimental Data on Linear Kinetics and the Formulation of Models," *J. Appl. Phys.* 27, 1361 (1956).

represents retention for the total body, which was obtained from (2) by summing the rows of (2), that is, it is the sum of all the body compartments.

$$Y(t) = \begin{pmatrix} 0.00473 & 0.0709 & 0.310 & 0.614 \\ 0.00354 & 0.0538 & 0.360 & -0.418 \\ 0.0544 & 0.787 & -0.656 & -0.186 \\ 0.676 & -0.696 & 0.0193 & 0.000927 \end{pmatrix} \begin{pmatrix} e^{-0.00320t} \\ e^{-0.164t} \\ e^{-4.54t} \\ e^{-26.7t} \end{pmatrix} . \quad (2)$$

$$R(t) = 0.738e^{-0.00320t} + 0.216e^{-0.164t} + 0.034e^{-4.54t} + 0.0115e^{-26.7t} . \quad (3)$$

As a test of this model, we employ the daily intake of Mg in reference man's diet of 0.34 g per day[3] and an absorption into blood from gut of 0.45,[1] as given by Avioli and Berman. In studies by Yun et al.[4] (the compound was not stated) on two human subjects, the values found are 0.53 to 0.93, higher than Avioli and Berman's value. Integrating over time, we obtain the equilibrium body burden

$$q = \int_0^\infty 0.34 \times 0.45 \times d\tau\, R(t - \tau) = 36 \text{ g} , \quad (4)$$

which is in agreement with reference man's burden of 29 g of Mg. Aikawa indicates that about 60% of this is in skeleton, 20% in muscle, and the remainder in other soft tissues. This is not a close estimate of the distribution obtained from the model, that is, 92% in one compartment, which might be identified with the skeleton, 7% in a second compartment (muscle), and only 1% in the other two compartments. It might be preferable to regard the compartment containing 92% of the body content as consisting not only of skeleton but also of portions of muscle and other soft tissues, and thus more nearly approximate the distribution of the stable element.

Figure 15.2 shows a revised model in which the long-term compartment is subdivided into two separate compartments. Two of these each receive 50% of $\lambda_{43}$ while one receives 60%, and the flow back $\lambda_{34}$ is the same for each one. This compartment model is the same as Avioli and Berman's when the two compartments 4′ and 4″ are combined. Then Eqs. (2) apply, and the fourth equation corresponds to the sum of compartments 4′ and 4″. This can be proved easily by writing out the linear differential equations and then summing Eqs. 4′ and 4″. The equations for the burden in the two additional compartments are

$$y_{4''}(t) = y_{4'}(t) = 0.50\,(0.676e^{-0.00320t} - 0.696e^{-0.164t} + 0.0193e^{-4.54t} + 0.000927e^{-26.7t}) = 0.50\, y_4(t) .$$

The radiation dose to the total soft tissues and skeleton is estimated with this model and the decay scheme data shown in Table 15.1. From the data on absorbed fractions of photon energy, we estimate the effective energy per disintegration to be, from Table 15.2 and adding the electron plus beta energies from $^{28}$Mg and $^{28}$Al, for skeleton

$$\mathcal{E}_{SK} = \begin{cases} 0.0474 \text{ MeV for source in soft tissues} \\ 1.566 \text{ MeV for source in skeleton} \end{cases}$$

while for soft tissue

$$\mathcal{E}_{ST} = \begin{cases} 1.803 \text{ MeV for source in soft tissues} \\ 0.275 \text{ MeV for source in skeleton} \end{cases}$$

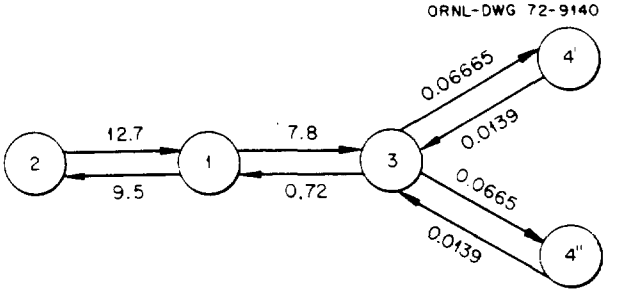


**Fig. 15.2. Revised compartment model for Mg metabolism.**

3. J. K. Aikawa, *The Role of Magnesium in Biologic Processes*, C. C. Thomas, Springfield, Ill., 1963, pp. 65, 67.

4. T. K. Yun, R. Lazzara, W. C. Black, J. J. Walsh, and G. E. Birch, "The Turnover of Magnesium in Control Subjects and in Patients with Idiopathic Cardiomyopathy and Congestive Heart Failure Studies with Magnesium-28," *J. Nucl. Med.* 7, 177 (1966).

In the above we assume that the short-lived $^{28}$Al undergoes decay in situ. Later, when more data on Al metabolism are available, we may not have to make this assumption.

Table 15.1. L. T. Dillman's decay scheme data[a] for $^{28}$Mg and $^{28}$Al

| Radiation | Percent per decay | Energy (MeV) |
|---|---|---|
| $^{28}$Mg: $T_r$ = 0.875 day; | | |
| $\beta$, average energy = 0.1586 MeV | | |
| $\gamma_1$ | 96.899 | 0.0310 |
| Internal conversion electrons | 3.101 | 0.0294 |
| $\gamma_2$ | 30.00 | 0.4000 |
| $\gamma_3$ | 30.00 | 0.9500 |
| $\gamma_4$ | 69.999 | 1.3500 |
| $KA_1$ x rays | 0.171 | 0.0015 |
| *KLL* Auger electrons | 2.587 | 0.0014 |
| *KLX* Auger electrons | 0.344 | 0.0015 |
| *LMM* Auger electrons | 5.688 | 0.0001 |
| $^{28}$Al: $T_r$ = 2.3 min; | | |
| $\beta$, average energy = 1.2392 MeV | | |

[a]Decay scheme data in files of Information Center for Internal Exposure, ORNL.

From Eq. (3) we obtain the residence time of $^{28}$Mg, $Q_x$, as 1.1 $\mu$Ci-days for the soft tissues and 0.063 $\mu$Ci-day for skeleton. Thus the dose commitment is

$$DE_{\text{bone}} = \frac{51}{7000}(1.6Q_{\text{bone}} + 0.047Q_{\text{soft tissues}})$$

$$\cong 0.0011 \text{ rad to bone per } \mu\text{Ci into blood}$$

and

$$DE_{\text{soft tissues}} = \frac{51}{63{,}000}(1.8Q_{\text{soft tissues}} + 0.3Q_{\text{bone}})$$

$$= 0.0017 \text{ rad to soft tissues per } \mu\text{Ci injection into blood.}$$

This compares favorably with the ICRP Publication 17[5] value for intravenous injection of 1 $\mu$Ci. The 37-kg muscle pool receives 2.7 millirads, while it is estimated the bone hot spots receive 2.1 millirads.

5. *Protection of the Patient in Radionuclide Investigations.* ICRP Publication 17, Pergamon, Oxford, 1971.

Table 15.2. Absorbed fractions of photon and electron (plus beta) energies $\phi_{T \leftarrow S}$ and specific absorbed energies for $^{28}$Mg and $^{28}$Al

| Radiation | Energy (MeV) | Specific absorbed fractions from target ← source[a] | | | | Effective energies, target ← source[b] (MeV) | | | |
|---|---|---|---|---|---|---|---|---|---|
| | | $\phi_{SKSK}$ | $\phi_{SKTB}$ | $\phi_{TBTB}$ | $\phi_{TBSK}$ | $\&_{SKSK}$ | $\&_{SKST}$ | $\&_{STSK}$ | $\&_{STST}$ |
| $\gamma_1$ | 0.031 | 0.7 | 0.19 | 0.78 | 0.85 | 0.021 | 0.00357 | 0.00014 | 0.0199 |
| $\gamma_2$ | 0.400 | 0.12 | 0.05 | 0.34 | 0.33 | 0.0144 | 0.00456 | 0.0252 | 0.0364 |
| $\gamma_3$ | 0.950 | 0.11 | 0.046 | 0.32 | 0.32 | 0.0314 | 0.00998 | 0.0599 | 0.0798 |
| $\gamma_4$ | 1.350 | 0.105 | 0.042 | 0.31 | 0.30 | 0.0992 | 0.0293 | 0.190 | 0.267 |
| $KA_1$ x ray | 0.0015 | 1 | 0 | 1 | 1 | 0.000003 | 0 | ~0 | 0 |
| Absorbed photon energy | | | | | | 0.166 | 0.0474 | 0.275 | 0.403 |

[a]These values were obtained from MIRD Suppl. No. 3, Pamphlet No. 5, 1969. The following identity is used to calculate the appropriate specific absorbed fractions $\phi$: TB stands for total body, SK for skeleton, and ST for soft tissues; SKTB means that the source is the total body and the target is the skeleton.

$\phi_{SKST} = 70/60\,\phi_{SKTB} - 10/60\,\phi_{SKSK}$,

$\phi_{STSK} = \phi_{TBSK} - \phi_{SKSK}$,

$\phi_{STST} = 70/60\,(\phi_{TBTB} - \phi_{SKTB}) - 10/60\,(\phi_{TBSK} - \phi_{SKSK})$.

In the above the masses of the skeleton (10 kg), the soft tissues (60 kg), and total body (70 kg) enter as weighting factors, for example, 70/60, etc.

This is obtained from the data in Table 15.1 on energy emitted times the appropriate specific absorbed fraction shown in the third column of the above table.